2012 IEEE International Conference on Robotics and Automation
RiverCentre, Saint Paul, Minnesota, USA
May 14-18, 2012

Extraction of Latent Kinematic Relationships Between Human Users and Assistive Robots

Jun Morimoto, Tomoyuki Noda and Sang-Ho Hyon

Abstract— **In this study, we propose a control method for movement assistive robots using measured signals from human users. Some of the wearable assistive robots have mechanisms that can be adjusted to human kinematics (e.g., adjustable link length). However, since the human body has a complicated joint structure, it is generally difficult to design an assistive robot which mechanically well fits human users. We focus on the development of a control algorithm to generate corresponding movements of wearable assistive robots to that of human users even when the kinematic structures of the assistive robot and the human user are different. We first extract the latent kinematic relationship between a human user and the assistive robot. The extracted relationship is then used to control the assistive robot by converting human behavior into the corresponding joint angle trajectories of the robot. The proposed approach is evaluated by a simulated robot model and our newly developed exoskeleton robot.**

I. INTRODUCTION

Assistive robots for patients and elderly people are seen as an important research topic in robotics; particularly movement assisting devices that have a wide variety of applications including rehabilitation. Therefore, development of movement assistive robots is becoming popular [1], [2], [3], [4], [5], [6], [7]. Hitherto, however, most of the works have focused on the development of hardware devices, while the software needed to control a movement assistive robot has not been intensively studied.

A significant difference in the requirements for controlling a movement assistive robot as opposed to other types of robots is that the robot needs to interact continuously and physically with humans. From a hardware development point of view, preparing adjustable mechanisms that can adapt to the size of the human user is important to coordinate properly the physical interaction between the robot and the human user. However, since a human's joint structure is complicated, it is generally difficult to design an assistive robot which mechanically well fits human users.

In this study, we propose a control method for movement assistive robots using measured signals from the human user. First, while the user is wearing the movement assistive robot, we simultaneously measure the joint angle trajectories of the human user and those of the robot. Next, we ascertain the kinematic relationship between user and robot movements. To extract the latent kinematic relationship, we use canonical correlation analysis (CCA) [8]. Since the human body has a complicated joint structure and cannot be tightly fixed to a movement assistive robot, finding the analytical kinematic relationship is difficult. Therefore, we propose extracting this relationship directly from the acquired data. However, a problem with finding the kinematic relationship is that both the human body and the movement assistive robot have many degrees of freedom. Thus, the number of parameters needed to represent the relationship between such systems with high-degrees of freedom can be large. On the other hand, human joint movements can be highly correlated (synergistic [9]) for a particular behavior. In this case, the estimated parameters may be overfitted for the acquired data and the generalization performance of the extracted relationship would be significantly worse. To cope with this overfitting problem, we propose using an ARD (auto relevance determination) approach [10]. More specifically, we use variational Bayesian canonical correlation analysis (VB-CCA) [11]. In this framework, we can select the correct number of dimensions to describe the relationship between a human user and the movement assistive robot from the acquired data.

In addition to finding the kinematic relationship, we propose using an electromyography (EMG) signal to control the movement assistive robot through the extracted kinematic relationship. The EMG signal can be used as a feedforward signal to control the movement assistive robot, while a goniometer attached to the human body is used for feedback control.

We evaluate how the combined system can be used to control a movement assistive robot using a simulated assistive robot model together with our newly develop exoskeleton robot (ATR eXoskeleton Robot, or XoR for short) (see also Fig. 1)[12].

II. EXTRACTION OF LATENT KINEMATIC RELATIONSHIPS

In this section, we introduce a method to extract the latent kinematic relationship through finding a shared state space between a human user and an assistive robot (see also Fig. 2). To extract the kinematic relationship, we apply canonical correlation analysis (CCA) to the simultaneously acquired movement data from the human user and the assistive robot. Throughout this paper, we define that the vector $\mathbf{x}$ denotes

J. Morimoto is with the Department of Brain Robot Interface, ATR Computational Neuroscience Labs, 2-2-2 Hikaridai, Seikacho, Sorakugun, Kyoto, JAPAN. xmorimo@atr.jp

T. Noda is with the Department of Brain Robot Interface, ATR Computational Neuroscience Labs, 2-2-2 Hikaridai, Seikacho, Sorakugun, Kyoto, JAPAN. t_noda@atr.jp

S. Hyon is with the Department of Brain Robot Interface, ATR Computational Neuroscience Labs, 2-2-2 Hikaridai, Seikacho, Sorakugun, Kyoto, JAPAN, and with Faculty of Science and Engineering, Ritsumeikan University, 1-1-1 Noji-Higashi, Kusatsu, Shiga, JAPAN. gen@fc.ritsumei.ac.jp

978-1-4673-1404-6/12/$31.00 ©2012 IEEE

Fig. 1. Our newly developed eXoskeleton Robot (XoR)[12]. Height: 1.5 m, Weight: 30 kg. XoR has ten degrees of freedom and six active joints. Each active joint uses a hybrid actuator composed of air muscle and an electric motor. XoR is designed to assist lower-limb movements in humans.

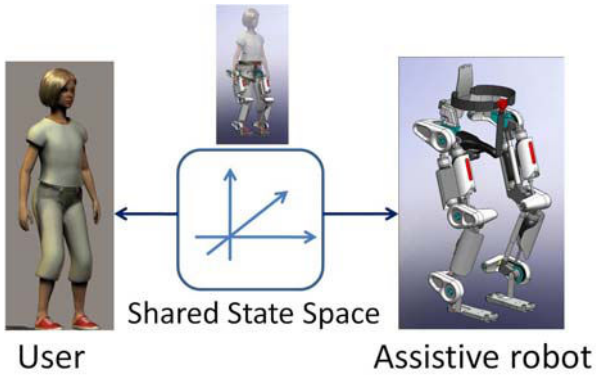

Fig. 2. Extracting the latent kinematic relationship through finding the shared state space between a human user and an assistive robot.

the state of the human user and the vector $\mathbf{y}$ denotes the state of the assistive robot.

A. Canonical Correlation Analysis (CCA)

Here, we briefly introduce canonical correlation analysis (CCA) [8], which can be used to extract the latent relationship between two random vectors.

We consider two random vectors $\mathbf{x}$ and $\mathbf{y}$, where the state vector of one observation is denoted by $\mathbf{x} \in X \subset \mathcal{R}^{d_\mathbf{x}}$ and the state vector of the other observation is denoted by $\mathbf{y} \in Y \subset \mathcal{R}^{d_\mathbf{y}}$. CCA derives directions $\mathbf{w_x}$ and $\mathbf{w_y}$ such that the correlation between two projected random variables $\mathbf{w_x x}$ and $\mathbf{w_y y}$ is maximized.

Thus, CCA can be formulated as an optimization problem in which the objective function is defined as

$$\rho = \max_{\mathbf{w_x},\mathbf{w_y}} \frac{\mathbf{w}_\mathbf{x}^T \Sigma_\mathbf{xy} \mathbf{w_y}}{\sqrt{\mathbf{w}_\mathbf{x}^T \Sigma_\mathbf{xx} \mathbf{w_x} \mathbf{w}_\mathbf{y}^T \Sigma_\mathbf{yy} \mathbf{w_y}}}. \quad (1)$$

where ρ is the correlation between projected values of both observations on canonical vectors, and Σ is the covariance. Since the solution of (1) is not affected by any rescaling of the projections, the optimization problem can be rewritten as:

$$\max_{\mathbf{w_x},\mathbf{w_y}} \mathbf{w}_\mathbf{x}^T \Sigma_\mathbf{xy} \mathbf{w_y} \quad (2)$$
$$\text{subject to} \quad \mathbf{w}_\mathbf{x}^T \Sigma_\mathbf{xx} \mathbf{w_x} = 1, \quad \mathbf{w}_\mathbf{y}^T \Sigma_\mathbf{yy} \mathbf{w_y} = 1.$$

This problem can be solved by finding eigenvectors for a generalized eigenvalue problem

$$\begin{pmatrix} 0 & \Sigma_\mathbf{xy} \\ \Sigma_\mathbf{yx} & 0 \end{pmatrix} \begin{pmatrix} \mathbf{w_x} \\ \mathbf{w_y} \end{pmatrix} = \rho \begin{pmatrix} \Sigma_\mathbf{xx} & 0 \\ 0 & \Sigma_\mathbf{yy} \end{pmatrix} \begin{pmatrix} \mathbf{w_x} \\ \mathbf{w_y} \end{pmatrix}. \quad (3)$$

B. Variational CCA

The probabilistic model of CCA was proposed in [13]. This model assumes that the two observed random vectors $\mathbf{x}$ and $\mathbf{y}$ are generated from the same latent vector $\mathbf{z}$:

$$\mathbf{x} = \mathbf{W_x z} + \boldsymbol{\eta}_\mathbf{x} \quad (4)$$
$$\mathbf{y} = \mathbf{W_y z} + \boldsymbol{\eta}_\mathbf{y}, \quad (5)$$

where $\mathbf{z} \in Z \subset \mathbf{R}^m$ and

$$P(\mathbf{z}) = \mathcal{N}(\mathbf{z}|\mathbf{0}, \mathbf{I}_m), \quad (6)$$
$$P(\boldsymbol{\eta}_\mathbf{x}) = \mathcal{N}(\boldsymbol{\eta}_\mathbf{x}|\mathbf{0}, \boldsymbol{\Sigma}_\mathbf{x}), \quad (7)$$
$$P(\boldsymbol{\eta}_\mathbf{y}) = \mathcal{N}(\boldsymbol{\eta}_\mathbf{y}|\mathbf{0}, \boldsymbol{\Sigma}_\mathbf{y}). \quad (8)$$

$\mathbf{I}_m$ is an m-dimensional identity matrix, $\Sigma_\mathbf{x}$ and $\Sigma_\mathbf{y}$ are covariance matrices.

We generally do not know how many latent variables, i.e., the number of elements m in the latent vector $\mathbf{z}$, are involved in explaining the two observed random vectors. The easiest way to determine the number of canonical correlations is simply to use the same number of dimensions as that of an observed vector with a smaller number of elements. However, if the true number of canonical correlations is smaller than the assumed number of dimensions, the standard CCA model can be overfitted for a particular set of sample data.

On the other hand, using this probabilistic CCA model, we can introduce a sparse prior to the model so that the number of canonical correlations can be automatically selected through a hierarchical Bayesian framework. This corresponds to ARD. To do this, we use the variational CCA proposed in [11]. Figure 3 shows a graphical model of the probabilistic CCA with a hierarchical Bayesian framework.

The joint distribution of the probabilistic CCA can be given as (see Fig. 3)

$$P(\mathbf{x}, \mathbf{y}, \mathbf{z}, \boldsymbol{\Theta}) = P(\mathbf{x}|\mathbf{z}, \mathbf{W_x}, \boldsymbol{\Sigma}_\mathbf{x}) P(\mathbf{y}|\mathbf{z}, \mathbf{W_y}, \boldsymbol{\Sigma}_\mathbf{y}) P(\mathbf{z}) P(\boldsymbol{\Theta}), \quad (9)$$

where the joint distribution of the parameters is:

$$P(\boldsymbol{\Theta}) = P(\mathbf{W_x}|\boldsymbol{\alpha}_\mathbf{x}) P(\mathbf{W_y}|\boldsymbol{\alpha}_\mathbf{y}) P(\boldsymbol{\alpha}_\mathbf{x}) P(\boldsymbol{\alpha}_\mathbf{y}) P(\boldsymbol{\Sigma}_\mathbf{x}) P(\boldsymbol{\Sigma}_\mathbf{y}). \quad (10)$$

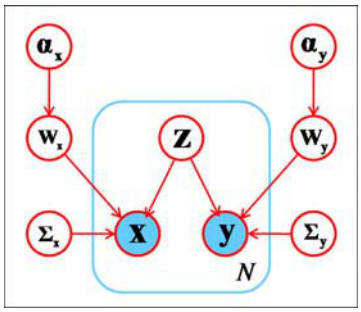

Fig. 3. Probabilistic CCA model with a hierarchical Bayesian framework. The shading of variables $\mathbf{x}$ and $\mathbf{y}$ implies that these variables can be observed (see also [14]). The rectangle labeled with N indicates that there are N observations. $\mathbf{z}$ is the latent variable. $\mathbf{W_x}$ and $\mathbf{W_y}$ are weight matrices. $\Sigma_\mathbf{x}$ and $\Sigma_\mathbf{y}$ are covariances of the random vectors $\mathbf{x}$ and $\mathbf{y}$, respectively. $\boldsymbol{\alpha}_\mathbf{x}$ and $\boldsymbol{\alpha}_\mathbf{y}$ determine the covariance of the weight matrices.

We use the conjugate priors as the prior distribution of the parameters:

$$P(\mathbf{W_x}|\boldsymbol{\alpha_x}) = \prod_j^{d_\mathbf{x}} \mathcal{N}(\mathbf{w}_\mathbf{x}^j|\mathbf{0}, (\mathrm{diag}\{\boldsymbol{\alpha}_\mathbf{x}\})^{-1}), \quad (11)$$

$$P(\mathbf{W_y}|\boldsymbol{\alpha_x}) = \prod_j^{d_\mathbf{y}} \mathcal{N}(\mathbf{w}_\mathbf{y}^j|\mathbf{0}, (\mathrm{diag}\{\boldsymbol{\alpha}_\mathbf{y}\})^{-1}), \quad (12)$$

$$P(\boldsymbol{\alpha_x}) = \prod_i^{m} \Gamma(\alpha_\mathbf{x}^i|a^0, b_i^0), \quad (13)$$

$$P(\boldsymbol{\alpha_y}) = \prod_i^{m} \Gamma(\alpha_\mathbf{y}^i|a^0, b_i^0), \quad (14)$$

$$P(\boldsymbol{\Sigma_x}) = \mathcal{W}(\boldsymbol{\Sigma_x}|\mathbf{K}_\mathbf{x}^0, \nu_\mathbf{x}^0), \quad (15)$$

$$P(\boldsymbol{\Sigma_y}) = \mathcal{W}(\boldsymbol{\Sigma_y}|\mathbf{K}_\mathbf{y}^0, \nu_\mathbf{y}^0), \quad (16)$$

where Γ is the Gamma distribution and $\mathcal{W}$ is the Wishart distribution (see [14] for more details). The hyper parameter that controls the sparseness of the weight vector is represented by $\boldsymbol{\alpha} = (\alpha^1, \ldots, \alpha^m)$.

Since integrations to derive the marginal distribution,

$$P(\mathbf{x}, \mathbf{y}) = \int P(\mathbf{x}, \mathbf{y}, \mathbf{z}, \boldsymbol{\Theta}) d\mathbf{z} d\boldsymbol{\Theta}, \quad (17)$$

are analytically intractable, we consider a variational approximation to the true posterior distribution by introducing the distribution $Q(\mathbf{z}, \boldsymbol{\Theta})$. The lower bound of the log marginal distribution is calculated as follows:

$$\begin{aligned} \ln P(\mathbf{x}, \mathbf{y}) &= \ln \int P(\mathbf{x}, \mathbf{y}, \mathbf{z}, \boldsymbol{\Theta}) d\mathbf{z} d\boldsymbol{\Theta} \\ &= \ln \int Q(\mathbf{z}, \boldsymbol{\Theta}) \frac{P(\mathbf{x}, \mathbf{y}, \mathbf{z}, \boldsymbol{\Theta})}{Q(\mathbf{z}, \boldsymbol{\Theta})} d\mathbf{z} d\boldsymbol{\Theta} \\ &\geq \int Q(\mathbf{z}, \boldsymbol{\Theta}) \ln \frac{P(\mathbf{x}, \mathbf{y}, \mathbf{z}, \boldsymbol{\Theta})}{Q(\mathbf{z}, \boldsymbol{\Theta})} d\mathbf{z} d\boldsymbol{\Theta} \\ &= \mathcal{L}(Q). \end{aligned} \quad (18)$$

We find that the difference between the log marginal distribution and the lower bound $\mathcal{L}(Q)$ can be represented by the Kullback-Leibler (KL) divergence between the true posterior and the selected distribution $Q(\mathbf{z}, \boldsymbol{\Theta})$ as

$$KL(Q||P) = \ln P(\mathbf{x}, \mathbf{y}) - \mathcal{L}(Q), \quad (19)$$

where the KL divergence is defined as

$$KL(Q||P) = -\int Q(\mathbf{z}, \boldsymbol{\Theta}) \ln \frac{P(\mathbf{z}, \boldsymbol{\Theta}|\mathbf{x}, \mathbf{z})}{Q(\mathbf{z}, \boldsymbol{\Theta})} d\mathbf{z} d\boldsymbol{\Theta}. \quad (20)$$

Since the marginal log likelihood is only determined by the observed data ($\mathbf{x}$ and $\mathbf{y}$) and is not a function of distribution Q, maximizing the lower bound $\mathcal{L}(Q)$ corresponds to minimizing the KL divergence between the true posterior and distribution Q. Thus, if we can find an analytically tractable distribution Q such that we can maximize the lower bound $\mathcal{L}(Q)$, the true posterior $P(\mathbf{z}, \boldsymbol{\Theta}|\mathbf{x}, \mathbf{y})$ can be efficiently approximated by distribution Q. To do this, we use the factorized distribution,

$$Q(\mathbf{z}, \boldsymbol{\Theta}) = Q(\mathbf{z}) Q(\mathbf{W_x}) Q(\mathbf{W_y}) Q(\boldsymbol{\alpha_x}) Q(\boldsymbol{\alpha_y}) Q(\boldsymbol{\Sigma_x}) Q(\boldsymbol{\Sigma_y}). \quad (21)$$

By maximizing the lower bound $\mathcal{L}(Q)$, distribution Q can be derived as follows:

$$Q(\mathbf{z}) = C_\mathbf{z} \exp \langle \ln P(\mathbf{x}, \mathbf{y}, \mathbf{z}, \boldsymbol{\Theta}) \rangle_{Q(\boldsymbol{\Theta})}, \quad (22)$$

$$Q(\boldsymbol{\Theta}_i) = C_{\boldsymbol{\Theta}_i} \exp \langle \ln P(\mathbf{x}, \mathbf{y}, \mathbf{z}, \boldsymbol{\Theta}) \rangle_{Q(\mathbf{z})Q(\boldsymbol{\Theta}_{k \neq i})}, \quad (23)$$

where $C_\mathbf{z}$ and $C_{\boldsymbol{\Theta}_i}$ are normalization constants. The brackets $< \cdot >_Q$ represent the expectation with respect to distribution Q. By considering (4)-(23), we find the factorized distribution Q as follows:

$$Q(\mathbf{z}) = \mathcal{N}(\mathbf{z}|\boldsymbol{\mu}_\mathbf{z}, \boldsymbol{\Sigma}_\mathbf{z}), \quad (24)$$

$$Q(\mathbf{w}_\mathbf{x}^j) = \mathcal{N}(\mathbf{w}_\mathbf{x}^j|\boldsymbol{\mu}_\mathbf{wx}^j, \boldsymbol{\Sigma}_\mathbf{wx}^j), \quad j = 1 \ldots d_\mathbf{x}, \quad (25)$$

$$Q(\mathbf{w}_\mathbf{y}^j) = \mathcal{N}(\mathbf{w}_\mathbf{y}^j|\boldsymbol{\mu}_\mathbf{wy}^j, \boldsymbol{\Sigma}_\mathbf{wy}^j), \quad j = 1 \ldots d_\mathbf{y}, \quad (26)$$

$$Q(\boldsymbol{\alpha}_\mathbf{x}^i) = \Gamma(\boldsymbol{\alpha}_\mathbf{x}^i|a_\mathbf{x}, b_\mathbf{x}^i), \quad i = 1 \ldots m, \quad (27)$$

$$Q(\boldsymbol{\alpha}_\mathbf{y}^i) = \Gamma(\boldsymbol{\alpha}_\mathbf{y}^i|a_\mathbf{y}, b_\mathbf{y}^i), \quad i = 1 \ldots m, \quad (28)$$

$$Q(\boldsymbol{\Sigma}_\mathbf{x}) = \mathcal{W}(\boldsymbol{\Sigma}_\mathbf{x}|\mathbf{K}_\mathbf{x}, \nu_\mathbf{x}), \quad (29)$$

$$Q(\boldsymbol{\Sigma}_\mathbf{y}) = \mathcal{W}(\boldsymbol{\Sigma}_\mathbf{y}|\mathbf{K}_\mathbf{y}, \nu_\mathbf{y}). \quad (30)$$

Then, the update rules for each parameter of the factorized distribution are given as:

$$\boldsymbol{\Sigma}_\mathbf{z} = \left(\mathbf{I} + \langle \mathbf{W}_\mathbf{x}^T \boldsymbol{\Sigma}_\mathbf{x} \mathbf{W}_\mathbf{x} \rangle + \langle \mathbf{W}_\mathbf{y}^T \boldsymbol{\Sigma}_\mathbf{y} \mathbf{W}_\mathbf{y} \rangle\right)^{-1}, \quad (31)$$

$$\boldsymbol{\mu}_\mathbf{z}^k = \boldsymbol{\Sigma}_\mathbf{z} \left[\mathbf{x}_k^T \langle \boldsymbol{\Sigma}_\mathbf{x} \rangle \langle \mathbf{W}_\mathbf{x} \rangle + \mathbf{y}_k^T \langle \boldsymbol{\Sigma}_\mathbf{y} \rangle \langle \mathbf{W}_\mathbf{y} \rangle\right]^T, \quad (32)$$

$k = 1, \ldots, N$, where N denotes the number of samples,

$$\nu_\mathbf{x} = \nu_\mathbf{x} + N, \quad (33)$$

$$\nu_\mathbf{y} = \nu_\mathbf{y} + N, \quad (34)$$

$$\mathbf{K}_\mathbf{x} = \mathbf{K}_\mathbf{x}^0 + \left\langle \sum_{k=1}^N (\mathbf{x}_k - \mathbf{W}\mathbf{z}_k)(\mathbf{x}_k - \mathbf{W}\mathbf{z}_k)^T \right\rangle, \quad (35)$$

$$\mathbf{K}_\mathbf{y} = \mathbf{K}_\mathbf{y}^0 + \left\langle \sum_{k=1}^N (\mathbf{y}_k - \mathbf{W}\mathbf{z}_k)(\mathbf{y}_k - \mathbf{W}\mathbf{z}_k)^T \right\rangle, \quad (36)$$

$$\boldsymbol{\Sigma}_\mathbf{wx}^j = \left[\mathrm{diag} < \boldsymbol{\alpha}_\mathbf{x} > + \sum_{k=1}^N \left(\langle \mathbf{z}_k \mathbf{z}_k^T \rangle \langle \boldsymbol{\Sigma}_\mathbf{x}^{j,j} \rangle\right)\right]^{-1}, \quad (37)$$

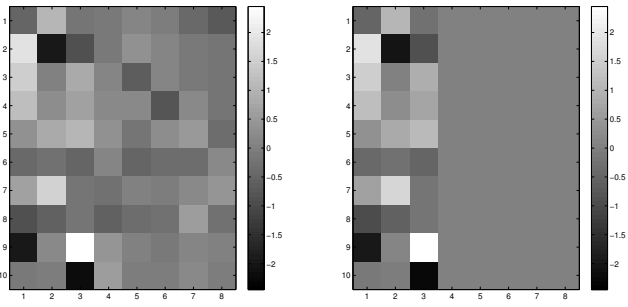

Fig. 4. Illustrative example: (left) standard CCA, (right) variational CCA. In the right figure, sparse projection matrix can be observed.

$$\boldsymbol{\Sigma}^j_{\mathbf{wy}}=\left[\text{diag} < \boldsymbol{\alpha}_{\mathbf{y}} > + \sum_{k=1}^{N} \left(\left\langle \mathbf{z}_k \mathbf{z}_k^T \right\rangle \left\langle \boldsymbol{\Sigma}^{j,j}_{\mathbf{y}} \right\rangle \right) \right]^{-1}, \tag{38}$$

$$\boldsymbol{\mu}^j_{\mathbf{wx}}=\boldsymbol{\Sigma}_{\mathbf{wx}} \sum_{k=1}^{N} \left[\mathbf{x}_k^T \left\langle \boldsymbol{\Sigma}^j_{\mathbf{x}} \right\rangle \left\langle \mathbf{z}_k \right\rangle^T - \left\langle \mathbf{z}_k \mathbf{z}_k^T \right\rangle \sum_{l \neq j}^{d_{\mathbf{x}}} \left\langle \mathbf{w}^l_{\mathbf{x}} \right\rangle^T \left\langle \boldsymbol{\Sigma}^{l,j}_{\mathbf{x}} \right\rangle \right], \tag{39}$$

$$\boldsymbol{\mu}^j_{\mathbf{wy}}=\boldsymbol{\Sigma}_{\mathbf{wy}} \sum_{k=1}^{N} \left[\mathbf{y}_k^T \left\langle \boldsymbol{\Sigma}^j_{\mathbf{y}} \right\rangle \left\langle \mathbf{z}_k \right\rangle^T - \left\langle \mathbf{z}_k \mathbf{z}_k^T \right\rangle \sum_{l \neq j}^{d_{\mathbf{y}}} \left\langle \mathbf{w}^l_{\mathbf{y}} \right\rangle^T \left\langle \boldsymbol{\Sigma}^{l,j}_{\mathbf{y}} \right\rangle \right], \tag{40}$$

$$a_{\mathbf{x}}=a^0 + \frac{d_{\mathbf{x}}}{2}, \tag{41}$$

$$a_{\mathbf{y}}=a^0 + \frac{d_{\mathbf{y}}}{2}, \tag{42}$$

$$b^i_{\mathbf{x}}=b^0_i + \frac{\left\langle ||\mathbf{W}^i_{\mathbf{x}}||^2 \right\rangle}{2}, \tag{43}$$

$$b^i_{\mathbf{y}}=b^0_i + \frac{\left\langle ||\mathbf{W}^i_{\mathbf{y}}||^2 \right\rangle}{2}, \tag{44}$$

where $\boldsymbol{\Sigma}^{j,j}$ denotes the j-th diagonal element of matrix $\boldsymbol{\Sigma}$, $\boldsymbol{\Sigma}^{l,j}$ denotes (l,j) element of matrix $\boldsymbol{\Sigma}$, $\boldsymbol{\Sigma}^j$ denotes the j-th column vector of matrix $\boldsymbol{\Sigma}$ and $\mathbf{W}^i$ denotes the i-th column vector of matrix $\mathbf{W}$.

C. Illustrative example

In this section we present an illustrative example of how CCA and variational CCA work. We consider two observation vectors $\mathbf{x} \in \mathbf{R}^8$ and $\mathbf{y} \in \mathbf{R}^{10}$, which are assumed to be generated from latent vector $\mathbf{z} \in \mathbf{R}^3$.

We randomly generated the latent vector $\mathbf{z}$ from the normal distribution in (6). $\boldsymbol{\Sigma}_{\mathbf{x}}$ and $\boldsymbol{\Sigma}_{\mathbf{y}}$ in (7) and (8), respectively, are unit covariance matrix. Each element of the projection matrices $\mathbf{W}_{\mathbf{x}}$ and $\mathbf{W}_{\mathbf{y}}$ is also generated from the normal distribution $\mathcal{N}(0,1)$.

By simply using CCA, we estimate the projection matrices $\mathbf{W}_{\mathbf{x}}$ and $\mathbf{W}_{\mathbf{y}}$ as shown in Fig. 4 (left). On the other hand, using variational CCA and as a result of ARD, we can find the sparse projection matrices as shown in Fig. 4 (right).

III. Joint angle prediction using EMG

So far we have focused on the problem of finding the latent kinematic relationship between the human user and the assistive robot. In this section, we consider the control problem that uses the derived kinematic relationship.

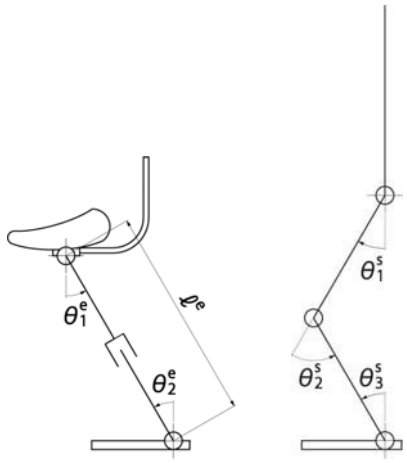

Fig. 5. Simplified simulation models for (left) an exoskeleton robot and (right) a human user. The exoskeleton robot model is composed of three links with one slider joint (l^e) and two revolve (rotational) joints (θ^e_1, θ^e_2). The human user model is composed of four links with three revolve joints ($\theta^s_1, \theta^s_2, \theta^s_3$).

As introduced in the previous section, we can find the state of the assistive robot that corresponds to the state of the human user through the derived shared state space. Thus, we can use the corresponding state of the assistive robot as the desired joint angles and angular velocities to control the robot using a proportional-derivative (PD) controller.

Generally, we need to use higher gains to achieve smaller tracking errors. However, it is not preferable to use very high gains for the PD controller since a human must wear the assistive robot. To reduce the tracking errors without using very high gain feedback, we can use predicted desired joint angles $\boldsymbol{\theta}$ and angular velocities $\dot{\boldsymbol{\theta}}$ as the feedforward control signal. Moreover, the predicted desired joint trajectory is necessary to assist human behaviors since the robot can start moving a bit earlier than initiation of a human behavior.

To generate the predicted desired joint angles and angular velocities, we use the EMG signals of human users [15], [16]. In this study, we use a linear prediction model:

$$\mathbf{x}(k+1) = \mathbf{A}\mathbf{x}(k) + \mathbf{B}\mathbf{u}(k), \tag{45}$$

where $\mathbf{x} = \left(\boldsymbol{\theta}, \dot{\boldsymbol{\theta}}\right)$ and $\mathbf{u} = (EMG_1, EMG_2, ..., EMG_n)$. Parameters $\mathbf{A}$ and $\mathbf{B}$ can be derived from the simultaneously measured joint angles $\boldsymbol{\theta}$, angular velocities $\dot{\boldsymbol{\theta}}$, and EMG data. Using the linear model is a popular approach for movement reconstruction (e.g., [17], [18]), and we also empirically find that the linear model is sufficient to reconstruct the movements considered in this study.

IV. Simulation

Here, we consider an assistive robot model, depicted in Fig. 5(left) and, a simplified human user model, depicted in Fig. 5(right). As shown in Fig. 5, these two models have different kinematic properties. The assistive robot model is composed of three links with one slider joint (l^e) and two revolve (rotational) joints (θ^e_1, θ^e_2). The human user model is composed of four links with three revolve joints ($\theta^s_1, \theta^s_2, \theta^s_3$).

In this simulation, we attempt to find the latent kinematic relationship between the human user and assistive robot models using variational CCA.

We assume that the user's feet are attached to the feet of the assistive robot and that the user takes the saddle. In other words, foot and hip positions are the same for the two models. We consider the sinusoidal movements of the horizontal hip position as shown in Fig. 6.

As depicted in Fig. 5, the state of the assistive robot is $\mathbf{y} = (l^e, \theta_2^e, \theta_3^e)$ and that of the human user is $\mathbf{x} = (\theta_1^s, \theta_2^s, \theta_3^s)$.

In this simulation study, we purely focus on the kinematic relationship and only consider joint angles.

Figure 7 shows the trajectories of the states of the human user and the robot as the hip position moves horizontally.

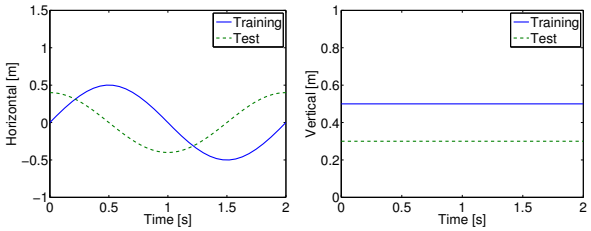

Fig. 6. (left) Horizontal and (right) vertical trajectories of hip positions for training data and test data.

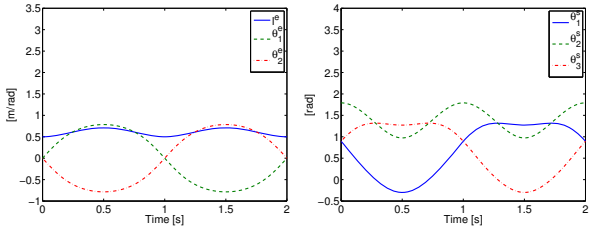

Fig. 7. Joint trajectories of (left) exoskeleton and (right) human user models.

We extract the latent kinematic relationship through finding the shared state space using variational CCA. In this simulation, by using the ARD property of variational CCA, we found a two-dimensional latent space with fewer dimensions than the state space of the human user or that of the assistive robot. Moreover, the variational CCA captures the number of dimension of the operational 2-D space only from the acquired data.

In the variational CCA model, we derive distributions of weight matrices $\mathbf{W_x}$ and $\mathbf{W_y}$, for generating the user state $\mathbf{x}$ and the robot state $\mathbf{y}$, respectively, from the latent state $\mathbf{z}$. Here we consider using mean matrices of the distirubutions $\bar{\mathbf{W}}_\mathbf{x}$ and $\bar{\mathbf{W}}_\mathbf{y}$, where $\bar{\mathbf{W}} = \left[\boldsymbol{\mu}^1, \boldsymbol{\mu}^2, \ldots, \boldsymbol{\mu}^d\right]^T$. The row vectors of the mean matrices are derived in (39) and (40). Simultaneously, we can derive the pseudo inverse of the mean weight matrix $\bar{\mathbf{W}}_\mathbf{x}^+$. Thus, we can derive the state of the assistive robot model $\mathbf{y}$ from the human user state $\mathbf{x}$ as

$$\mathbf{y} = \bar{\mathbf{W}}_\mathbf{y} \bar{\mathbf{W}}_\mathbf{x}^+ \mathbf{x}. \tag{46}$$

In Fig. 8, we compare the estimated trajectory of the robot model using (46) with the actual trajectory that can be derived analytically from knowledge of the parameters of kinematics models. The plots in Fig. 8 show that the estimated trajectories are almost same as the actual. This results indicate that the latent kinematic relationship is correctly estimated.

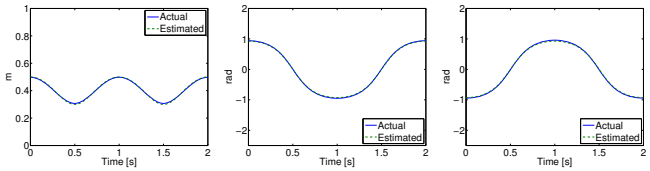

Fig. 8. Reconstructed joint trajectories $(l^e, \theta_1^e, \theta_2^e)$. Estimated trajectories are almost same as actual.

V. Finding Shared State Space using Exoskeleton Robot

In this section, we consider using our newly developed exoskeleton assistive robot XoR. XoR is designed to assist lower-limb movements of humans. XoR has ten degrees of freedom and six active joints. Each active joint use a hybrid actuator composed of air muscle and electric motor. By using the hybrid actuator, we can develop a light weight robot with high power actuation [12], [19], [20].

A. Finding shared state space

First, a human subject rides on the assistive robot and generates squat movements. We measure the joint angles and angular velocities of the human subject and the assistive robot simultaneously using encoders on the robot and goniometers attached to the human subject.

The state of the human subject $\mathbf{x} = (\theta_1^s, \theta_2^s, \theta_3^s)$ is the same as that depicted in Fig. 5(right). The state of the assistive robot XoR $\mathbf{y} = (\theta_1^e, \theta_2^e, \theta_3^e)$ is illustrated in Fig. 9. Note that this kinematics model is different from the model presented in Fig. 5(left. Figure 10 shows the squat movement of the exoskeleton robot XoR. Having found the shared state space between the human subject and the assistive robot, we derive the corresponding state of the assistive robot to the human subject state using (46).

B. Predicting state of human subject using EMG signals

As discussed in Section III, we predict the future state of the human subject using EMG signals. We measured

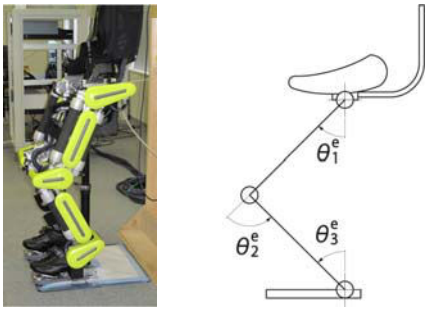

Fig. 9. Simulation model of our newly developed exoskeleton robot XoR.

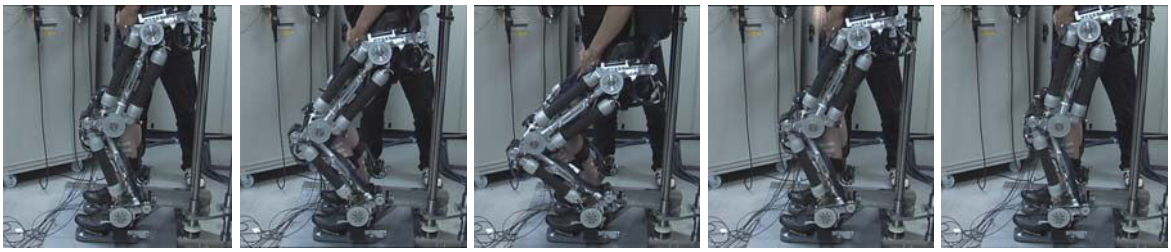

Fig. 10. Simultaneous acquisition of joint angle data for the exoskeleton robot XoR and the human user.

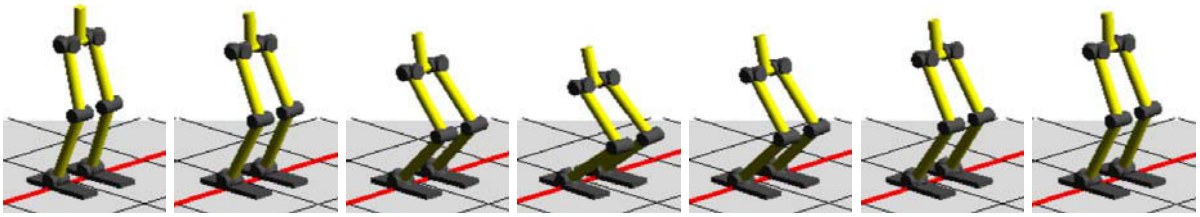

Fig. 11. Generated squat movement of the exoskeleton robot model.

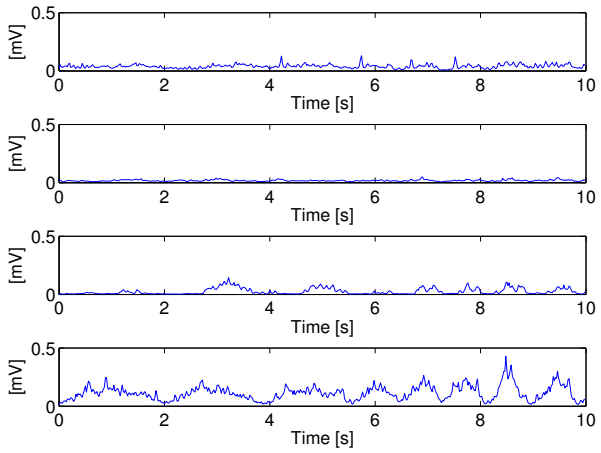

Fig. 12. EMG signals. Each plot, from top to bottom, shows EMG signal of Quadriceps femoris, Tensor fasciae latate, Gluteus medius, and Tibialis anterior, respectively.

activity in four muscles (Quadriceps femoris, Tensor fasciae latate, Gluteus medius, and Tibialis anterior) (see Fig. 12) to predict the joint angles and angular velocities as in (45). The measured EMG signals were rectified and low-pass filtered with 10 Hz cut-off. The input to the linear system in (45) is $\mathbf{u} = (EMG_1, EMG_2, EMG_3, EMG_4)$. The predicted state is used as the desired input to the PD controller:

$$\tau_i = K_p(\theta_i^d - \theta_i^s) + K_d(\dot{\theta}_i^d - \dot{\theta}_i^s), \tag{47}$$

where τ_i is the torque output and θ_i^d is the predicted state for the i-th joint. $K_p = 1000$ and $K_d = 100$ are the servo gains.

C. Application to simulated exoskeleton robot model

To evaluate the proposed approach, we applied this control scheme to the simulated XoR model. We used a dynamical model for the assistive robot.

In Fig. 13, we evaluated the tracking errors between the actual movement of the robot and the simulated movement of the robot model. The mean-squared error, when applying the predicted desired state generated by EMG, was 1.8×10^{-3}. If we simply used the current joint angles and angular velocities of the human subject, the mean-squared error was 2.1. These results show the benefit of using the predicted desired states of human users to control assistive robots.

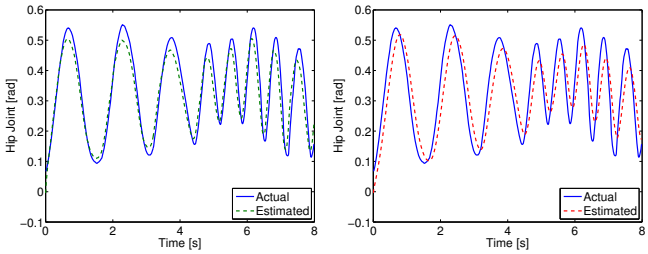

Fig. 13. Comparison of tracking errors at hip joints: (left) with EMG, (right) without EMG.

VI. CONCLUSIONS

In this study, we extracted the latent kinematic relationships between human users and assistive robots. Using the extracted relationship, we can efficiently transfer the movement intention of a human user to the assistive robot through the derived kinematic relationship.

We evaluated the proposed approach in a simulated environment. We also found the kinematic relationship between a human subject and the newly developed exoskeleton assistive robot XoR. The measured EMG and the extracted kinematic relationship were used to control the simulated XoR model. Then, we showed that we were able to control the XoR model by using the latent kinematic relationship and the EMG signal. We used the simple linear model to predict joint angles and angular velocities from EMG data. To cope

with wider variety of movements, we may need to use a nonlinear model [21]. We empirically figured out that the selected four muscles were useful for the prediction. As a next step, we will consider to develop an automatic muscle selection method.

As future studies, we combine the proposed framework with the pattern-generator-based biped locomotion controller [22] to support biped walking movements.

ACKNOWLEDGMENTS

This research is the result of "Brain Machine Interface Development" carried out under the Strategic Research Program for Brain Sciences by the Ministry of Education, Culture, Sports, Science and Technology of Japan. This work was partially supported by Grant-in-Aid for Scientific Research on Innovative Areas: Prediction and Decision Making 23120004.

REFERENCES

[1] S. Jacobsen, "On the Development of XOS, a Powerful Exoskeletal Robot," in *2007 IEEE/RSJ International Conference on Intelligent Robots and Systems, Plenary Talk*, 2007.

[2] H. Kazerooni and A. C. nad R. Steger, "That Which Does Not Stabilize, Will Only Make Us Stronger," *International Journal of Robotics Research*, vol. 26, no. 1, pp. 75–89, 2007.

[3] K. Suzuki, M. G. Kawamoto, H. Hasegarwa, and Y. Sankai, "Intension-based walking support for paraplegia patients with Robot Suit HAL," *Advanced Robotics*, vol. 21, no. 12, pp. 1441–1469, 2007.

[4] S. K. Au, P. Dilworth, and H. Herr, "An ankle-foot emulation system for the study of human walking biomechanics," in *IEEE International Conference on Robotics and Automation*, 2006, pp. 2939–2945.

[5] H. Kobayashi, A. Takamitsu, and T. Hashimoto, "Muscle Suit Development and Factory Application," *International Journal of Automation Technology*, vol. 3, no. 6, pp. 709–715, 2009.

[6] G. Yamamoto and S. Toyama, "Development of Wearable-Agri-Robot-Mechanism for Agricultural Work," in *IEEE/RSJ International Conference on Intelligent Robots and System*, 2009, pp. 5801–5806.

[7] T. Kagawa and Y. Uno, "Gait pattern generation for a power-assist device of paraplegic gait," in *The 18th IEEE International Symposium on Robot and Human Interactive Communication*, 2009, pp. 633–638.

[8] H. Hotelling, "Relations between two sets of variates," *Biometrika*, vol. 28, pp. 321–377, 1936.

[9] N. A. Bernstein, *On Dexterity and Its Development*. New York: Psychology Press, 1996.

[10] R. M. Neal, "Bayesian Learning for Neural Networks," in *Lecture Notes in Statistics 118*. New York: Springer, 1996.

[11] C. Wang, "Variational Bayesian Approach to Canonical Correlation Analysis," *IEEE Transaction on Neural Networks*, vol. 18, no. 3, pp. 905–910, 2007.

[12] S. Hyon, J. Morimoto, T. Matsubara, T. Noda, and M. Kawato, "XoR: Hybrid Drive Exoskeleton Robot That Can Balance," in *IEEE/RSJ International Conference on Intelligent Robots and Systems*, 2011.

[13] F. R. Bach and M. I. Jordan, "A probabilistic interppretation of canonical correlation analysis," Technical Report of the Department of Statistics, University of California, Berkeley, Tech. Rep., 2005.

[14] C. M. Bishop, *Pattern Recognition and Machine Learning*. NY, USA: Springer, 2006.

[15] Y. Koike and M. Kawato, "Estimation of dynamic joint torques and trajectory formation from surface electromyography signals using a neural network model," *Biological Cybernetics*, vol. 73, no. 4, pp. 291–300, 1995.

[16] P. Artemiadis and K. Kyriakopoulos, "EMG-based teleoperation of a robot arm in planar catching movements using ARMAX model and trajectory monitoring techniques," in *IEEE International Conference on Robotics and Automation*, 2006, pp. 3244–3249.

[17] T. Kitamura, N. Tsujiuchi, and T. Koizumi, "Hand motion estimation by EMG signals using linear multiple regression models," in *International Conference of IEEE Engineering in Medicine and Biology Society*, 2006, pp. 1339–1342.

[18] P. K. Artemiadis and K. J. Kyrakopoulos, "EMG-Based COntrol of a Robot Arm Using Low-Dimensional Embeddings," *IEEE Transactions on Robotics*, vol. 26, no. 2, pp. 393–398, 2010.

[19] H. Hisa, Y. Tanaka, and S. Minimisawa, "Rotation Type of Electric and Pneumatic Hybrid Actuator," in *Nihon Kikai Gakkai Nenji Taikai Koen Ronbunshu (in Japanese)*, 2007, pp. 311–312.

[20] I. Sardellitti, J. Park, D. Shin, and O. Khatib, "Air muscle controller design in the distributed macro-mini (DM2) actuation approach," in *IEEE/RSJ International Conference on Intelligent Robots and Systems*, 2007, pp. 1822–1827.

[21] C. E. Rasmussen and C. K. I. Williams, *Gaussian Processes for Machine Learning*. Cambridge, MA: The MIT Press, 2006.

[22] J. Morimoto, G. Endo, J. Nakanish, and G. Cheng, "A Biologically Inspired Biped Locomotion Strategy for Humanoid Robots: Modulation of Sinusoidal Patterns by a Coupled Oscillator Model," *IEEE Transaction on Robotics*, vol. 24, no. 1, 2007.